



Since January 2020 Elsevier has created a COVID-19 resource centre with free information in English and Mandarin on the novel coronavirus COVID-19. The COVID-19 resource centre is hosted on Elsevier Connect, the company's public news and information website.

Elsevier hereby grants permission to make all its COVID-19-related research that is available on the COVID-19 resource centre - including this research content - immediately available in PubMed Central and other publicly funded repositories, such as the WHO COVID database with rights for unrestricted research re-use and analyses in any form or by any means with acknowledgement of the original source. These permissions are granted for free by Elsevier for as long as the COVID-19 resource centre remains active.



# Investigating the structure-activity relationship of marine polycyclic batzelladine alkaloids as promising inhibitors for SARS-CoV-2 main protease (M<sup>PRO</sup>)

Alaa M. Elgohary<sup>a</sup>, Abdo A. Elfiky<sup>a,\*\*</sup>, Florbela Pereira<sup>b</sup>, Tarek Mohamed Abd El-Aziz<sup>c,d</sup>, Mansour Sobeh<sup>e</sup>, Reem K. Arafa<sup>f,g</sup>, Amr El-Demerdash<sup>h,i,\*</sup>

<sup>a</sup> Department of Biophysics, Faculty of Sciences, Cairo University, Giza, 12613, Egypt

<sup>b</sup> LAQV-REQUIMTE, Department of Chemistry, NOVA School of Science and Technology, Universidade Nova de Lisboa, 2829-516, Caparica, Portugal

<sup>c</sup> Department of Zoology, Faculty of Sciences, Minia University, El-Minia, 61519, Egypt

<sup>d</sup> Department of Cellular and Integrative Physiology, University of Texas Health Science Centre at San Antonio, San Antonio, TX, 78229, USA

<sup>e</sup> AgroBioSciences Department, Mohammed VI Polytechnic University (UM6P), Ben Guerir, Morocco

<sup>f</sup> Drug Design and Discovery Laboratory, Helmy Institute for Medical Sciences, Zewail City of Science and Technology, Giza, 12578, Egypt

<sup>g</sup> Biomedical Sciences Program, University of Science and Technology, Zewail City of Science and Technology, Giza, 12578, Egypt

<sup>h</sup> Department of Biochemistry and Metabolism, The John Innes Centre, Norwich Research Park, Norwich, NR4 7UH, UK

<sup>i</sup> Division of Organic Chemistry, Department of Chemistry, Faculty of Sciences, Mansoura University, Mansoura, 35516, Egypt

## ARTICLE INFO

### Keywords:

SARS-CoV-2

Batzelladines

Molecular docking

Molecular dynamics

Guanidine alkaloids

Marine sponges

SARs

## ABSTRACT

Over a span of two years ago, since the emergence of the first case of the novel coronavirus (SARS-CoV-2) in China, the pandemic has crossed borders causing serious health emergencies, immense economic crisis and impacting the daily life worldwide. Despite the discovery of numerous forms of precautionary vaccines along with other recently approved orally available drugs, yet effective antiviral therapeutics are necessarily needed to hunt this virus and its variants. Historically, naturally occurring chemicals have always been considered the primary source of beneficial medications. Considering the SARS-CoV-2 main protease (M<sup>PRO</sup>) as the duplicate key element of the viral cycle and its main target, in this paper, an extensive virtual screening for a focused chemical library of 15 batzelladine marine alkaloids, was virtually examined against SARS-CoV-2 main protease (M<sup>PRO</sup>) using an integrated set of modern computational tools including molecular docking (MDock), molecule dynamic (MD) simulations and structure-activity relationships (SARs) as well. The molecular docking predictions had disclosed four promising compounds including batzelladines H-I (8–9) and batzelladines F-G (6–7), respectively according to their prominent ligand-protein energy scores and relevant binding affinities with the (M<sup>PRO</sup>) pocket residues. The best two chemical hits, batzelladines H-I (8–9) were further investigated thermodynamically through studying their MD simulations at 100 ns, where they showed excellent stability within the accommodated (M<sup>PRO</sup>) pocket. Moreover, SARs studies imply the crucial roles of the fused tricyclic guanidinic moieties, its degree of unsaturation, position of the *N*-OH functionality and the length of the side chain as a spacer linking between two active sites, which disclosed fundamental structural and pharmacophoric features for efficient protein-ligand interaction. Such interesting findings are greatly highlighting further *in vitro/vivo* examinations regarding those marine natural products (MNPs) and their synthetic equivalents as promising antivirals.

## 1. Introduction

Over the span of seven decades, marine natural products (MNPs) and their synthetic congeners have been revitalised as a vigorous respiratory and robust platform for global pharmaceutical industry and drug led

discovery programmes [1]. Indeed, in 1950, Bergmann and his co-workers reported the first two marine compounds spongothymidine and spongouridine from the Caribbean marine sponge *Cryptotethya crypta* [2–4]. Twenty years later, they have been synthetically optimized to furnish the first two clinically approved marine drugs, commercially known as cytarabine (Cytosar-U®, Depocyst®, approved by FDA in

\* Corresponding author. Department of Biochemistry and Metabolism, the John Innes Centre, Norwich Research Park, Norwich, NR4 7UH, UK.

\*\* Corresponding author.

E-mail addresses: [dr\\_abdo@cu.edu.eg](mailto:dr_abdo@cu.edu.eg), [abdo@sci.cu.edu.eg](mailto:abdo@sci.cu.edu.eg) (A.A. Elfiky), [Amr.El-Demerdash@jic.ac.uk](mailto:Amr.El-Demerdash@jic.ac.uk), [a\\_eldemerdash83@mans.edu.eg](mailto:a_eldemerdash83@mans.edu.eg) (A. El-Demerdash).

1969 for cancer treatment) and vidarabine (Vira-A®, approved by FDA in 1976 as antiviral) [5–8]. Intriguingly, by 2022, successful seventeen

### Abbreviations

<b>ADC</b>	Antibody-Drug Conjugate
<b>ADME</b>	Absorption, distribution, metabolism, and excretion
<b>COVID-19</b>	Coronavirus disease 2019
<b>SARS-CoV-2</b>	severe acute respiratory syndrome-coronavirus 2
<b>MBAs</b>	Marine Batzelladine Alkaloids
<b>MNPs</b>	Marine Natural Products
<b>M<sup>Pro</sup></b>	Main Protease
<b>MDock</b>	Molecular Docking
<b>MD</b>	Molecular Dynamic Simulations
<b>SARs</b>	Structure-Activity Relationships
<b>VMD</b>	Visual Molecular Dynamics
<b>RMSD</b>	Root Mean Square Deviation
<b>MM-GBSA</b>	Molecular Mechanics-Generalized Born Surface Area
<b>UFF</b>	Universal Force Field
<b>SASA</b>	Solvent Accessible Surface Area

marine-derived drugs have been clinically approved for markets for the treatment of numerous medical and life induced challenges, in addition to twenty other candidates, which are currently being investigated in different preclinical trials. Indeed, in 2004, the peptide toxin,  $\omega$ -conotoxin MVIIA, known commercially as ziconotide (Prialt®), was approved for the treatment of severe pains. In the same year, a mixture of two ethyl esters of fish-derived  $\omega$ -3 polyunsaturated fatty acids, eicosapentanoic acid (EPA), and docosahexanoic acid (DHA) were marketed as (Lovaza®) by GSK and approved by FAD for reducing serum triglycerides.

Further two marine-based drugs were commercialized including (Vascepa®, pure EPA) produced by Amarin and (Epanova®, mix of three  $\omega$ -3 polyunsaturated fatty acids) manufactured by AstraZeneca were approved by the FAD in 2013–2014 respectively for the treatment of hypertriglyceridemia. In 2010, Eribulin Mesylate E7389, (Halave®) marketed by Eisai Pharmaceuticals, is a synthetic derivative based on the marine natural polyketide halichondrin B, was approved by the FAD for the treatment of metastatic breast cancer. In 2011, brentuximab vedotin (Adcetris®) marketed by Millennium Pharmaceuticals, is an antibody-drug conjugate (ADC) based on the marine natural peptide dolastatin 10, was approved for the treatment of Hodgkin maglinant lymphoma.

Later, in 2015, Ecteinascidin 743 (trabectedin, Yondelis®) commercialized by PharmaMar was the first approved anticancer directly derived from a marine natural product (MNP) and used for the treatment of soft tissue sarcoma and ovarian cancer. Additionally, Panobinostat (Farydak®), is a small synthetic derivative of an indole containing hydroxamic acid, was approved by the FAD in 2015 for the treatment of various forms of cancer particularly the myeloma one.

In 2018, Plitidepsin (Aplidin®), a small depsipeptide produced by PharmaMar was approved for the treatment of numerous cancer forms including multiple myeloma, leukemia and lymphoma. In 2019, Polatuzumab vedotin (DCDS-4501A) (Polivy®) commercialized by Genentech/Roche is a further ADC based on the marine natural peptide dolastatin 10 was approved for the treatment of various form of cancer including non-Hodgkin lymphoma, chronic lymphocytic and leukemia.

Further five marine derive compounds were introduced to markets and approved as anticancers for treatment of different forms of carcinoma, namely as [Enfortumab Vedotin, (Padcev®), by Astellas Pharma & Seattle Genetics, approved in 2019], [Lurbinectedin, (Zepzelca®) by PharmaMar, approved in 2020], [Belantamab-Mafodotin-blmf,

(Blenrep®) by GSK, approved in 2020], [Disitamab Vedotin, (Aidix®) by Remegen Biosciences, approved in 2021] and [Tisotumab vedotin-tftv, (Tivdak®) by Seagen, approved in 2021] [8–15]. Likely, such unique habitat presents thousands of new and novel compounds that are being disclosed each year from different marine organisms like sponges, soft corals, tunicates, algae, and microbes [16–21].

Along the discovery side, numerous chemical synthetic efforts are being expressed for the led optimization purposes towards a panel of structurally diverse marine compounds for various biomedical applications particularly as antiviral, anticancer, and against other nighligated diseases. Bearing such successful stories that imply the vast capacity of marine-derived natural products as a versatile hotspot for mining promising drugs leads that feature unprecedented structural and biological diversifications [22–24]. Recently in 2021–2022, several research reports highlighted plitidepsin, a small cyclic peptide previously isolated from the tunicate *Aplidium albicans* and originally approved as anticancer to disclose very promising *in vitro* antiviral activity against SARS-CoV-2 with IC<sub>90</sub> = 0.88 nM and might be a strong drug candidate that gives a hope for future treating of COVID-19 [25–28].

Marine batzelladines alkaloids (MBAs) is one fascinating class of a broad family of polycyclic guanidine-derived alkaloids which exclusively are restricted to the marine origin [29]. Chemically, they feature two main fused guanidinic portions linking together via an ester functionality, where a principle tricyclic system named clathriadic acid is assembled to another clathriadic acid or a crambescine bicyclic moiety [30]. Biogenetically, those marine alkaloids are supposed to be generated via sequential modes of cyclization between a polyketide-derived chain and a putative guanidine precursor along with different oxidation degrees to afford such complex metabolites [29,31–33].

Batzelladines derived alkaloids are known to display a vast array of biological activities like cytotoxicity, antimicrobial, antimalarial, anti-infective, anti-leishmanial and anti-parasitic [29]. Interestingly, a notable number of naturally occurring batzelladines and their synthetic analogues displayed powerful antiviral activities, including [batzelladines A-E (1–5) as anti-HIV-1], [batzelladine F–I, (6–9), inducers of p56lck-CD4 dissociation], [batzelladine K–N (10–13) and dehydrobatzelladine C (14) as anti-HIV-1 and anti-AIDS] and [Norbatzelladine L (15) as anti-HSV-1 [34–41].

Furthermore, Bewley and co-workers reported an extensive evaluation for a synthetic library of 28 batzelladine congeners for their ability to inhibit HIV-1 envelope-mediated cell-cell fusion. The authors studied the structure-activity relationships where it could imply up and downgrading the inhibition activity compared with natural batzelladines. Moreover, they suggested preferential lowest energy modelling studies for the inhibitors linked to the CD4 binding site on gp120 [42].

In order to find convenient therapeutic targets for the Mpro and since 2012 and onwards, therapeutic target database (TTD) a versatile online platform was initiated and mainly committed for recapping huge therapeutic information concerning almost 4500 targets/14500 drugs and their target validation information, quantitative structure activity relationships (Q-SARs) and clinical and pre-clinical trials [43–45].

Recently, numerous conformation-based drug screening and protein binder studies have been successfully verified to SARS-CoV-2. Yang and co-workers designed a structure-based discovery approach to identify of novel nonpeptide inhibitors which are targeting SARS-CoV-2 (M<sup>Pro</sup>) [46]. Moreover, they shaped a computational-based design for nanobodies against the angiotensin-converting enzyme 2 (ACE2) of SARS-CoV-2 [47].

Interestingly, Wang *et al.*, reported SYNBP: a global online platform for synthetic binding proteins for research, diagnosis and therapeutic purposes [48]. Recently, Zhang *et al.*, highlighted using advanced bioinformatic approaches which revealed the existence of significant microRNAs and their significant role for the protein-protein interactions between SARS-CoV-2 and the host benefit viral development during COVID-19 infection cycle [49,50].

Considering the central role of SARS-CoV-2 M<sup>pro</sup>, along with the powerful antiviral activities of the MNPs under investigation and as a part of our continuous program to identify pharmacologically active MNPs [51–54] with adequate antiviral potentiality against SARS-CoV-2 (COVID-19 pandemic) [55–57], herein we comprehensively exploring virtually the SARs of a focused library of fifteen marine batzelladine alkaloids against the dimeric form of SARS-CoV-2 (M<sup>pro</sup>) using an integrated package of advanced computational tools including (MDock), (MD) simulations and (SARs). These methods have been used to predict novel potential inhibitors of the protease and spike of SARS-CoV-2 and to understand the mechanism of action of different compounds such as neurotransmitters [58–62].

## 2. Material and methods

### 2.1. Preparation of the screening library and protein structure

The ChemDraw was utilized to draw the compounds and saved as MOL files [63]. Using Avogadro 1.2 software, ligand structures were converted to 3D (PDB files) and optimized by the universal force field (UFF) [64,65]. Further optimization was performed utilizing the parameterization method 6 (PM6) of SCIGRESS 3.0 software, followed by infra-red calculations at the same level of the semi-empirical method [66]. The positive control ligands O6K and N3 were also optimized using the same protocol after retrieval from the PDB structures 6Y2G and 6LU7, respectively [67,68]. Finally, all the ligands were prepared for docking by AutoDock tools 1.5.6 software [69]. Charges (Kollman and Gasteiger) were added while the PDBQT files of the ligands were saved for the docking calculations. Meanwhile, the M<sup>pro</sup> structure (PDB ID: 6Y2G) was separately prepared for the MD simulations and the MDock studies. We utilize this structure as it resembles the dimer configuration of the protein that was reported to be the active form of the polymerase, and it also has the O6K inhibitor associated with its active site pocket. Additionally, the 6LU7 structure has the N3 inhibitor bound to the M<sup>pro</sup> but it is a monomer. The best hits in our study are based on the average binding affinities calculated by AutoDock Vina on five different conformations of the M<sup>pro</sup> after MDS, representing the five different clusters of the trajectories of the protein. We performed the docking on five different conformations of M<sup>pro</sup> after dynamics simulation to remove any biased excreted by the rigid structure.

### 2.2. Molecular docking (MDock)

After clustering, five representative conformations, representing the different clusters, were prepared for the docking study using AutoDock Tools software. AutoDock Vina 1.2.2 [70] was used to dock the ligands to the protein active site defined by H41 and C145 as reported in a previous study [68]. During the docking calculations for all ligands, a flexible ligand in a flexible active site was maintained. The search box was set to cover the dyad H41 and C145 with size 30 × 30 × 30 Å<sup>3</sup> centered at (25.2, 46.0, 40.6) Å.

### 2.3. Molecular dynamics (MD) simulations

MD simulation of the M<sup>pro</sup> structure was performed by the NAMD 2.13 software utilizing CHARMM 36 force field [71,72]. The calculations were performed for 100 ns over the SHAHEEN HPC platform in the King Abdullah University for Science and Technology (KAUST), Saudi Arabia (project no. 1482). The simulation was performed in the TIP3P water model at 1 atm, and 310 K with NaCl added for the protein-water solution to be of a total concentration of 154 mM [73,74]. Periodic boundary condition was utilized with a cubic simulation box. After the simulation, the trajectories were clustered using UCSF Chimera software 1.14 and analyzed, as will be shown in the results section using VMD 1.9.3 software and in-house codes [75,76]. After the binding energy calculations, we ranked the ligands according to their binding energies

to (M<sup>pro</sup>). The best two ligand-M<sup>pro</sup> complexes (8-M<sup>pro</sup> and 9-M<sup>pro</sup>) and the O6K-M<sup>pro</sup> complex were subjected to another 100 ns MD simulations run with the same protocol. After the run, the Molecular Mechanics-Generalized Born Surface Area (MM-GBSA) was calculated using Amber tools to deconvolute the binding affinity as a per-residue contribution [77].

### 2.4. In-silico prediction of physicochemical properties, pharmacokinetic and toxicity profiles

The pharmacokinetic properties of the fifteen compounds in our screening library were calculated using the SWISS-ADME platform (<https://www.swissadme.ch>, accessed on February 04, 2022). The physicochemical properties predicted here were lipophilicity, reported as Log Po/w (WLOGP); water solubility class; and blood-brain barrier (BBB) penetration, in addition to pan-assay interference alerts (PAINS) [78,79].

The potential toxicity profiles of these compounds were predicted using the pkCSM online webtool (<http://biosig.unimelb.edu.au/pkcsim/prediction>, accessed on February 04, 2021) to predict the safety of these small molecules upon ingestion in human and animal models, with respect to toxicological effects on hERG-I inhibition [80].

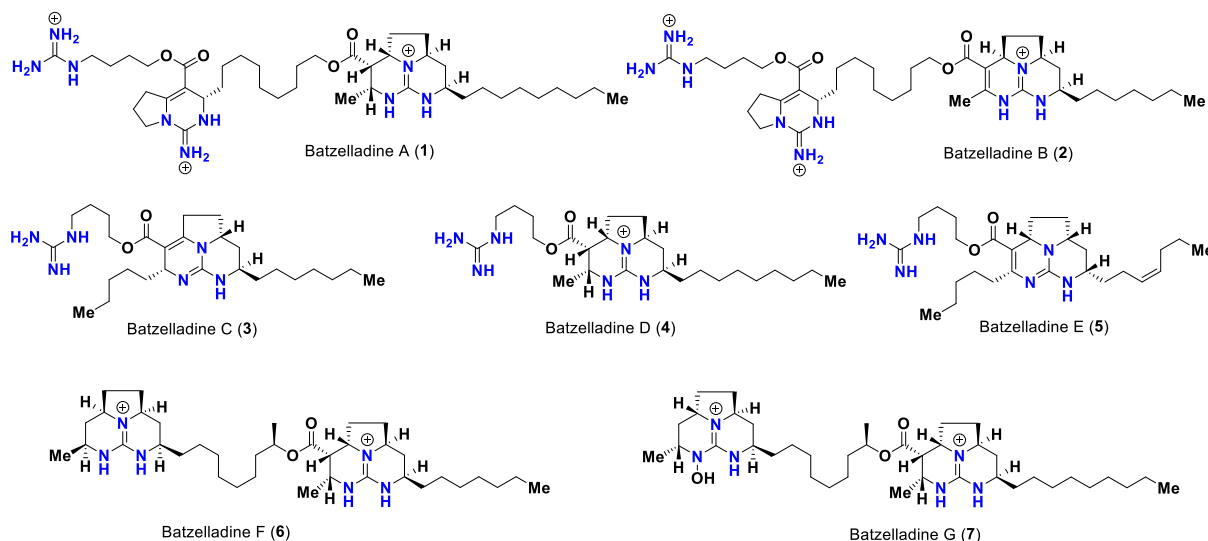
### 2.5. Identification of polycyclic marine batzelladine alkaloids (MBAs)

A focused library of fifteen batzelladines guanidine alkaloids (1–15) were previously reported from several marine sponges, belonging to the genera *Batzella*, *Clathria* and *Monanchora* (Schemes 1–2). For comprehensive detailed isolations and structural characterizations, see El-Demerdash et al. [29,81].

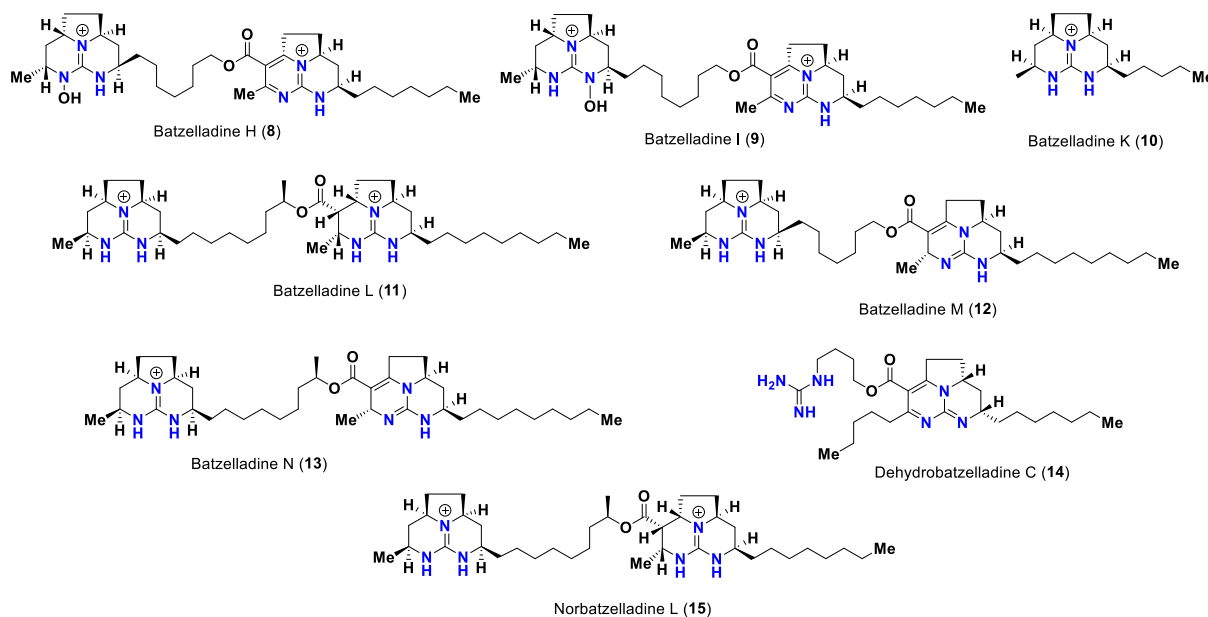
## 3. Results and discussions

### 3.1. Molecular docking (MDock) and binding energies studies

In this study, we studied fifteen marine polycyclic batzelladine alkaloids against SARS-CoV-2 M<sup>pro</sup> *in silico*, aiming to evaluate their binding energies and binding mode to the active site of M<sup>pro</sup>. Before discussing the compounds' binding energies, we represent the analysis curves for the MD simulations of the Apo M<sup>pro</sup> of the SARS-CoV-2 system (a dimer) using VMD software and some in-house analysis codes. Fig. 1A shows the Root Mean Square Deviation (RMSD) in Å (blue line), the Radius of Gyration (RoG) in Å (orange line), and the Surface Accessible Surface Area (SASA) in Å<sup>2</sup> (gray line). As reflected from the curves, the system was equilibrated during the first 10 ns of the simulation with an RMSD value of 1.8 Å. Additionally, the RoG and SASA values (26.0 Å and 27100 Å<sup>2</sup>, respectively) and patterns indicate system equilibration during the simulation period. Simultaneously, the total number of H-bonds present in the protein was found to be stable during the simulation period, as shown in Fig. 1B, with an average number of the total H-bonds of 924 (in the protein dimer). The per-residue Root Mean Square Fluctuations (RMSF) in Å is demonstrated in Fig. 1C, where the two chains of the M<sup>pro</sup> are shown in different colors. The active site dyads H41 and C145 are indicated in the RMSF curves at minimum fluctuations (RMSF >1 Å). During the simulation, there are no identified high fluctuations regions (all RMSF >2.26 Å). On the other hand, there are a few moderate fluctuation regions, in addition to the C-terminal arm (RMSF <1.40 Å), such as; T45-Y54 (red), G71-N72 (magenta), Y154-D155 (orange), R222-T225 (yellow), and N274-R279 (blue). These regions are depicted both on the RMSF curves by the colored pointers and on the structure by the colored cartoons. The figure shows that the moderate fluctuating regions are apart from the active site dyads (shown in black sticks). These regions are mainly loops connecting the secondary structures and hence are higher in flexibility compared to the other regions of M<sup>pro</sup>. The N-terminals of the two polypeptide chains are immersed in the protein core, so they have low flexibility (RMSF >1 Å).



Scheme 1. Reported antiviral batzelladines (1–7).



Scheme 2. Reported antiviral batzelladines (8–15).

In contrast, the C-terminal of chain 2 (magenta RMSF) freely protrudes from the protein surface and hence has higher fluctuations (RMSF <math><2.0 \text{ \AA}</math>).

A redocking experiment is essential in testing the docking protocol quality, as such the co-crystallized ligand **O6K** was retrieved from the crystal structure of  $M^{PTO}$  (PDB ID: 6Y2G) and docked to the protein dimer. PyMOL software was utilized to superpose the docked complex to the solved structure. The root-mean-square displacement (RMSD) between the complex and the solved structure was  $0.899 \text{ \AA}$ , where the number of fitted atoms was 1437, indicating high structural similarities (see [supplementary Fig. 1](#)). [Fig. 2A](#) shows the average binding affinities calculated utilizing five different conformations of the  $M^{PTO}$  after the 100 ns MD simulation. The error bars represent the standard deviation. The positive controls (**O6K** and **N3**) are shown in red columns, while the best two compounds (batzelladines **H–I**, **8–9**) are in green. Additionally, [Fig. 2B](#) displays the hydrophobic contacts (dashed-gray lines), which represent the interactions established between the ligands (orange sticks) and the  $M^{PTO}$  residues (blue sticks). As reflected from [Fig. 2A](#), the

average binding energies for most of the compounds under investigation are in good agreement with the positive controls, with compound **10** (batzelladine **K**) as an exception having a significantly low affinity against the  $M^{PTO}$  active site ( $-5.46 \pm 0.30 \text{ kcal/mol}$ ). For the rest of the compounds, the average binding energies ranged from  $-7.12 \pm 0.60$  (**8**) down to  $-6.22 \pm 0.37$  (**14**) kcal/mol, while for the positive control, binding energies were found to be  $-7.36 \pm 0.34 \text{ kcal/mol}$  and  $-6.36 \pm 0.31 \text{ kcal/mol}$  for **O6K** and **N3**, respectively.

The established interactions upon docking to the best representative complexes (having near average binding energy values) are listed in [Table 1](#) (see [supplementary Fig. 2](#)). Notably, the hydrophobic contact is the most reported interaction type, with few H-bonds formed in some complexes. For example, the **O6K**- $M^{PTO}$  complex formed the highest number of interactions, represented by eight hydrophobic contacts and 4 H-bonds. Concurrently with [Fig. 2](#), the **O6K**- $M^{PTO}$  complex reported the lowest average binding energy value ( $-7.36 \pm 0.34 \text{ kcal/mol}$ ). On the other hand, the **10**- $M^{PTO}$  complex showed the highest (worst) average binding energy value ( $-5.46 \pm 0.30 \text{ kcal/mol}$ ) and has only four



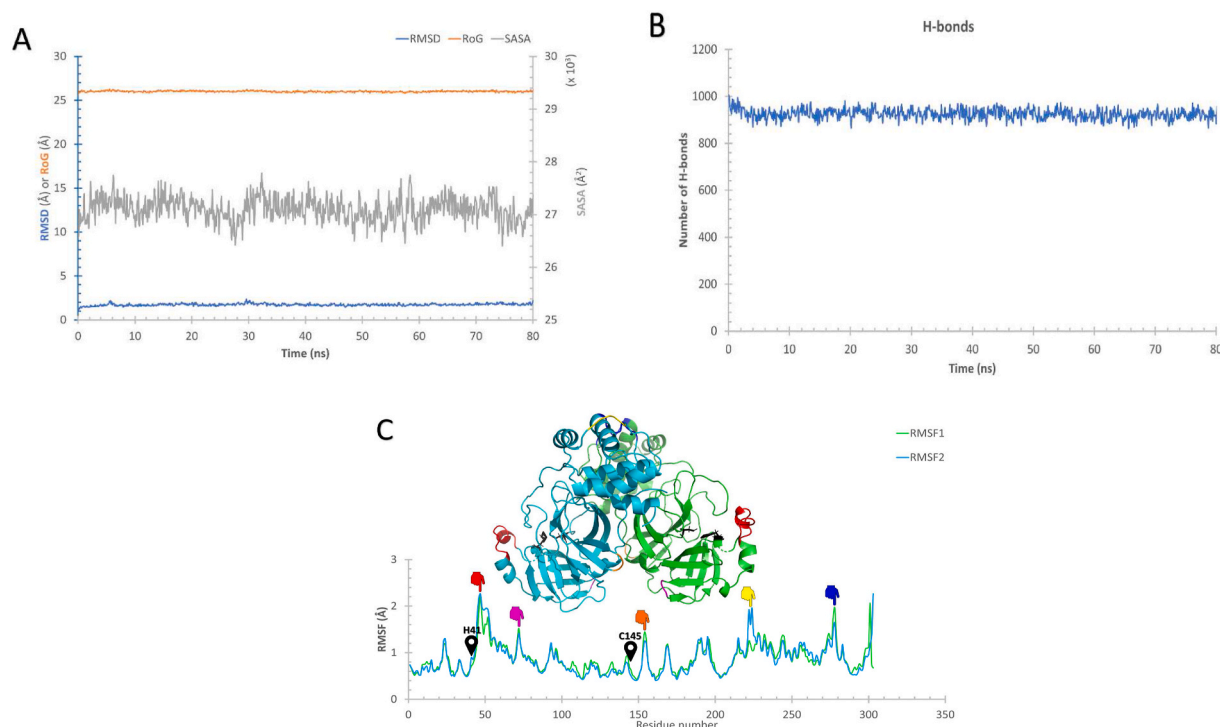


**Fig. 1.** Molecular Dynamics Simulation trajectory analysis for the Apo-M<sup>PRO</sup>. **A):** The Root-mean-square deviation (RMSD) (blue) in Å, Radius of Gyration (RoG) (orange) in Å, and Surface Accessible Surface Area (SASA) (gray) in Å<sup>2</sup>, versus the simulation time in ns. **B):** The total number of the H-bonds versus the simulation time. **C):** The per-residue Root-mean-square fluctuations (RMSF) in Å for the two chains of the dimeric M<sup>PRO</sup>.

hydrophobic contacts. The two complexes **8-M<sup>PRO</sup>** and **9-M<sup>PRO</sup>** are amongst the compounds of the highest number of formed interactions, showing 6 and 7 hydrophobic contacts, corresponding to their average binding energy values ( $-7.12 \pm 0.60$  and  $-7.0 \pm 0.28$  kcal/mol, respectively).

The residues in the M<sup>PRO</sup> that most frequently take part in interactions with the ligands are E166 (12 hydrophobic contacts and 6 H-bonds), M165 (13 hydrophobic contacts), and Q189 (12 hydrophobic contacts and one H-bond). Moreover, some other residues have moderate potential to interact with the ligands, including the active site residue, C145 (8 hydrophobic contacts and one H-bond), N142 (5 hydrophobic contacts and 3 H-bond), M49 (7 hydrophobic contacts), P168 (6 hydrophobic contacts), F140 (5 hydrophobic contacts), L167 (4 hydrophobic contacts and one H-bond), and Q192 (3 hydrophobic contacts and two H-bonds) (see Table 1).

Noteworthy, the interaction of S1 residue (red-colored in Table 1) in the Chain B of the M<sup>PRO</sup> dimer is involved, forming H-bonds with **O6K**, **1**, **3**, **4**, and **14**. This is reflected in the RMSF curve (Fig. 1C), as intramolecular contacts stabilize the N-terminal region. This highlights the importance of the dimeric form during the studying of M<sup>PRO</sup> inhibitors.

### 3.2. Molecular dynamic (MD) studies

Fig. 3 shows the MD simulation analysis of the **O6K-M<sup>PRO</sup>** (blue), **8-M<sup>PRO</sup>** (orange), and **9-M<sup>PRO</sup>** (gray). The three complexes are stable based on the RMSD (A), RoG (B), SASA (C), and the total number of H-bonds (D) curves versus the simulation time (ns). The RMSD curves indicate equilibration of the three systems after 30 ns with average RMSD values of about 2.25 Å. Additionally, the numbers of RoG, SASA, and H-bonds are averaged around 26 Å, 28200 Å<sup>2</sup>, and 940, respectively. The per-residue RMSF for the chain A and chain B (Fig. 4) is plotted for the Apo (red) and **O6K-M<sup>PRO</sup>** (blue), **8-M<sup>PRO</sup>** (orange), and **9-M<sup>PRO</sup>** (gray) complexes. The ligands are bound to the Chain A of the M<sup>PRO</sup>, which reflects the differences in the RMSF curves. Three regions show a significant difference between chain A and chain B of the M<sup>PRO</sup> in the RMSF.

The first region around residue 119 (dashed red rectangle) shows 3-fold higher fluctuations for the **8-M<sup>PRO</sup>** and **9-M<sup>PRO</sup>** than the Apo and the **O6K-M<sup>PRO</sup>**. The second region lies around residue 144 (dashed green rectangle) shows 1.5-fold higher fluctuations for the **8-M<sup>PRO</sup>** and **9-M<sup>PRO</sup>** compared to the Apo and the **O6K-M<sup>PRO</sup>**. On the other hand, the third region lies around residue 196 (dashed blue rectangle) and shows 1.5-fold higher fluctuations for the **8-M<sup>PRO</sup>** than the Apo, **O6K-M<sup>PRO</sup>**, and **9-M<sup>PRO</sup>**.

Fig. 3F shows the ligand RMSD versus the simulation time for the **O6K**, **8**, and **9-M<sup>PRO</sup>** complexes. As reflected in the figure, the best complex in ligand stability was the **8-M<sup>PRO</sup>**, as the ligand RMSD was stable (RMSD >9 Å) during the simulation period of 100 ns. This is not observed in the case of **O6K**- and **9-M<sup>PRO</sup>** complexes that have RMSD values of up to 126 Å and 102 Å, respectively. This reflects the instability of these ligands during the MD simulation.

To further elucidate each residue's binding energy (kcal/mol) contribution, we calculated the MM-GBSA of the two best complexes, **8-M<sup>PRO</sup>** and **9-M<sup>PRO</sup>**. Table 2 shows the per-residue decomposition of the binding energy contribution and the different energy term contributions for the total binding energy ( $\Delta G_{TOTAL}$ );  $\Delta E_{VDW}$ ,  $\Delta E_{ELE}$ ,  $\Delta G_{GB}$ ,  $\Delta G_{SA}$ ,  $\Delta G_{GAS}$ , and  $\Delta G_{SOLV}$ . The highest contribution for the residues of the M<sup>PRO</sup> for the two ligands **8** and **9** are listed in bold E166 ( $-13.39$  kcal/mol) and P168 ( $-2.01$  kcal/mol) in **8-M<sup>PRO</sup>** complex and D248 ( $-2.50$  kcal/mol) in the **9-M<sup>PRO</sup>** complex. Additionally, the ligands (LIG) have a high binding energy contribution in both complexes ( $-7.48$  and  $-2.48$  kcal/mol, for **8-M<sup>PRO</sup>** and **9-M<sup>PRO</sup>**, respectively).

Meanwhile, the residues M165, H172, L167, and F304 moderately contributed to the binding of batzelladine H (**8**) to M<sup>PRO</sup> with binding energy values of  $-0.87$ ,  $-0.75$ ,  $-0.67$ , and  $-0.47$  kcal/mol, respectively. These residues line near the active site, and due to the size of the ligands, they can help in masking the dyads (see supplementary Fig. 3). While the residues P252, I249, F294, and V297 contributed to the binding of batzelladine I (**9**) to M<sup>PRO</sup> with binding energy values of  $-1.28$ ,  $-1.05$ ,  $-0.73$ , and  $-0.44$  kcal/mol, respectively. Conversely, S302 (red-bold colored residue) has a negative contribution (positive

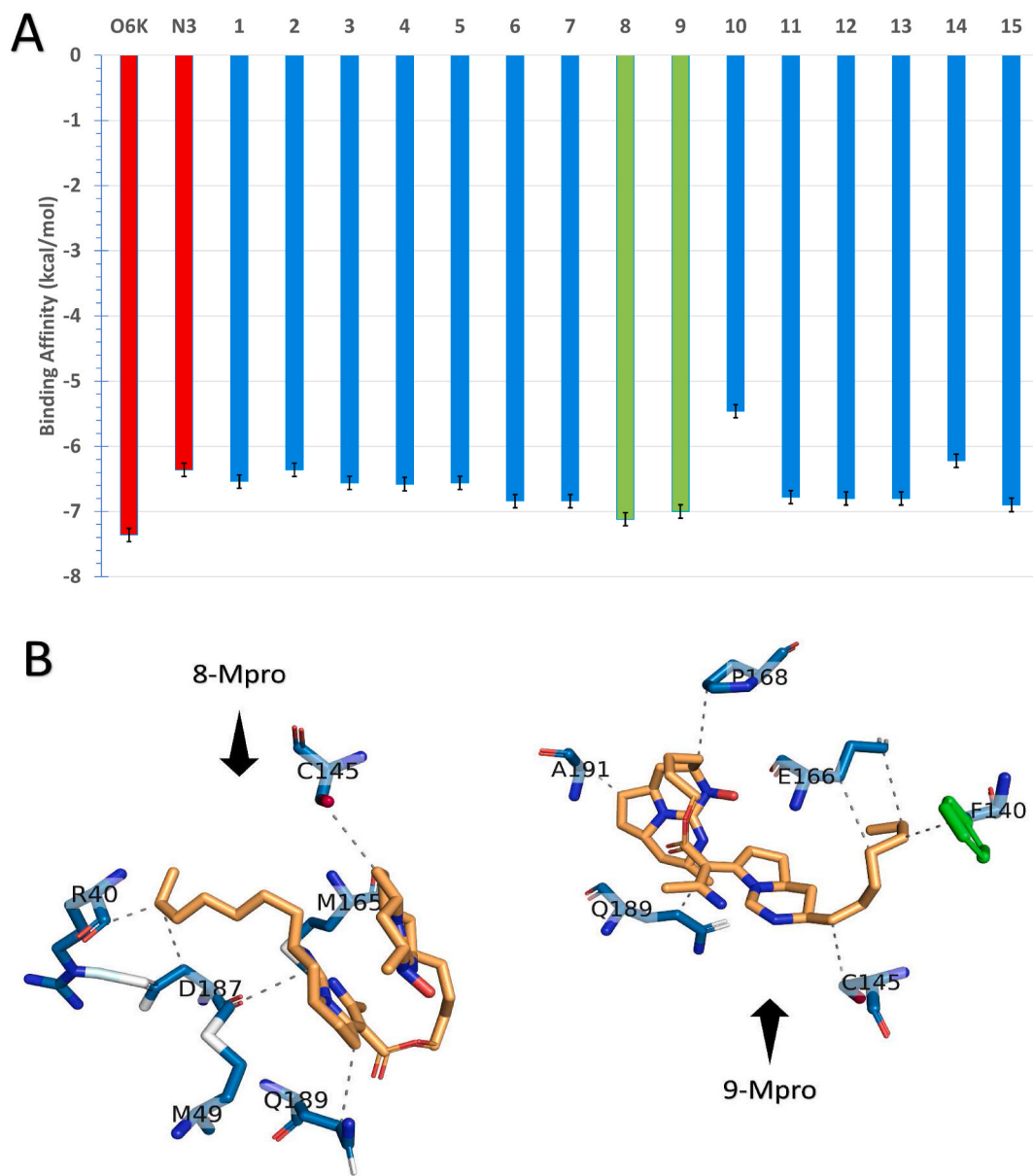


**Fig. 2.** **A):** The average binding energies of the tested compounds (1–15) and the positive controls O6K and N3 (red columns) retrieved from the structures (PDB IDs: 6Y2G and 6LU7, respectively). The best two compounds (8 and 9) are shown in green. **B):** Binding mode of the best two compounds (8 and 9) depicted by PyMOL software, where orange and blue sticks represent the ligands and the protein residues, respectively. Dashed-gray lines represent the hydrophobic contacts.

**Table 1**

The detailed interactions established upon docking the O6K, N3, and marine compounds (1–15) against the SARS-CoV-2 M<sup>PRO</sup> (PDB ID: 6Y2G, Chain A) retrieved from PLIP webserver. Red residues represent the residues that interact with the second chain of M<sup>PRO</sup> (Chain B).

Ligand	Hydrophobic Interactions		Hydrogen Bonds	
	No.	Residues involved	No.	Residues involved
O6K	4	N142, M165, D187 and Q189	8	<b>S1</b> , <b>H41</b> , G143, S144, <b>C145</b> , H164, and E166(2)
N3	3	T25, T26, and P168	2	H164 and E166
1	4	N142, <b>C145</b> , P168, and Q189	3	<b>S1(2)</b> and N142
2	4	M49, F140, M165, and E166	2	L167 and Q189
3	7	L27, P39, M49(2), <b>C145</b> , E166, and Q189	5	<b>S1</b> , L141(3), and N142
4	2	T25 and S46	3	<b>S1</b> , N142, and E166
5	5	M49, F140, M165, E166, and P168	3	E166 and Q192(2)
6	7	<b>C145</b> , M165(2), E166, L167, Q189, and Q192		
7	7	T25, M165, E166(2), L167, P168, and Q189	1	G143
8	6	R40, M49, <b>C145</b> , M165, D187, and Q189		
9	7	F140, <b>C145</b> , E166(2), P168, Q189, and A191		
10	4	F140, M165, E166, and Q189		
11	5	S46, F140, N142, and E166(2)		
12	3	L167, Q189, and Q192	1	E166
13	6	T26, N142, <b>C145</b> , M165(2), and Q189	1	T26
14	7	M49, N142, <b>C145</b> , M165, E166, P168, and Q189	2	<b>S1(2)</b>
15	7	M49, <b>C145</b> , M165(2), L167, Q189, and Q192		

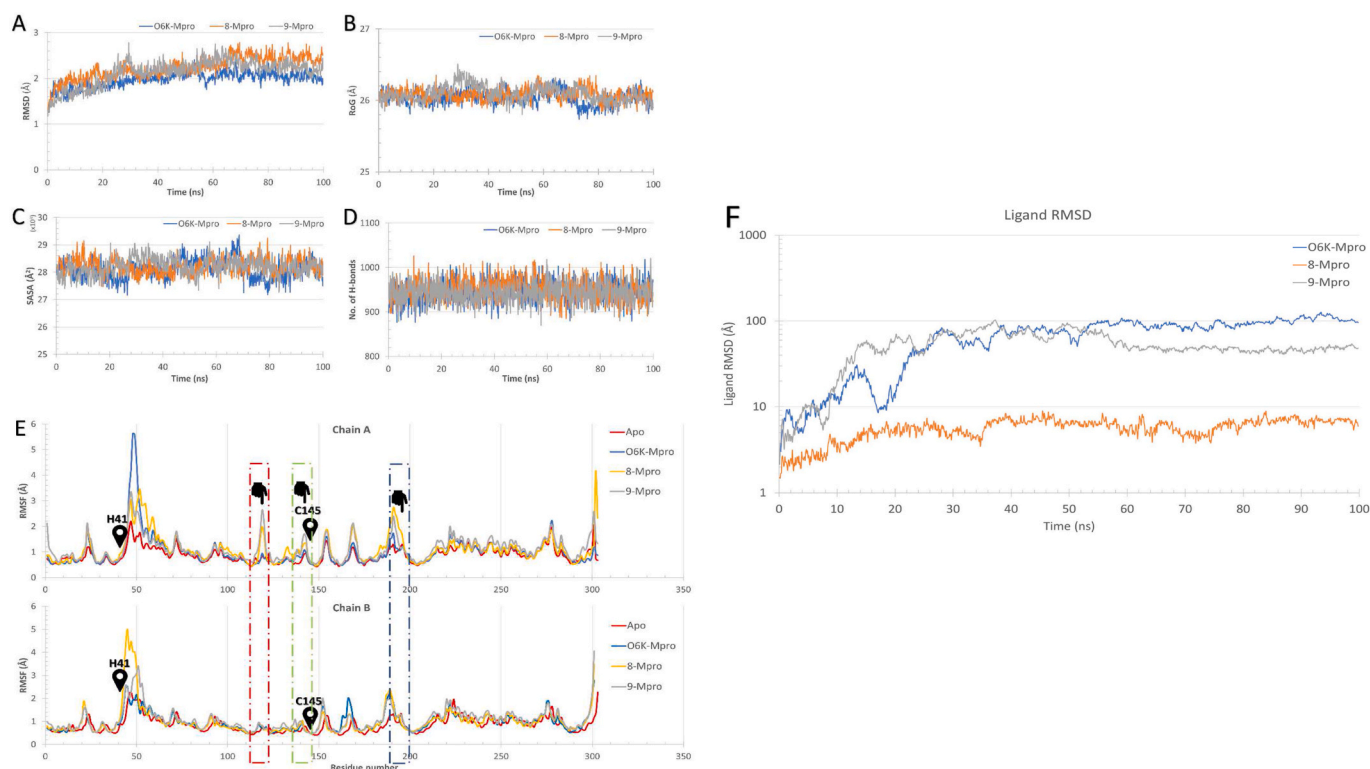


**Fig. 3.** Molecular dynamics simulation data analysis for O6K-M<sup>PRO</sup>, 8-M<sup>PRO</sup>, and 9-M<sup>PRO</sup> complexes. (A), (B), (C), and (D) show the RMSD, RoG, SASA, and H-bonds for the O6K-M<sup>PRO</sup> (blue), 8-M<sup>PRO</sup> (orange), and 9-M<sup>PRO</sup> (gray) complexes versus the simulation time in ns. (E) shows the per-residue RMSF from the two chains A (upper) and B (lower) of M<sup>PRO</sup> in the Apo form (red), O6K-M<sup>PRO</sup> complex (blue), 8-M<sup>PRO</sup> complex (orange), and 9-M<sup>PRO</sup> complex (gray). Active dyads and high fluctuating regions are marked on the curves as illustrated in the text. (F) The ligands RMSD (Å) versus the simulation time (ns) for the dynamics of O6K-M<sup>PRO</sup> (blue), 8-M<sup>PRO</sup> (orange), and 9-M<sup>PRO</sup> (gray) complexes.



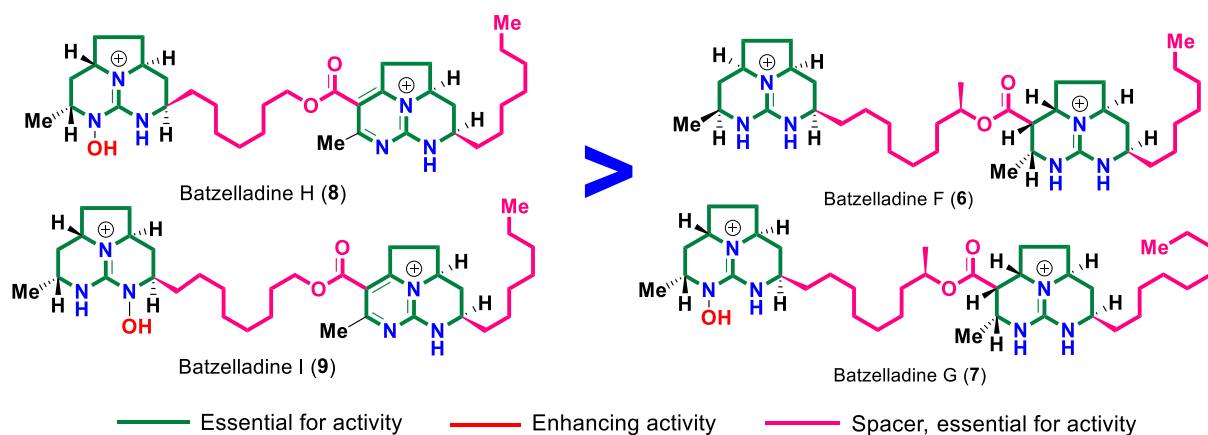


Fig. 4. Chemical structure of the most promising derivatives (6–7) and (8–9) with regarded to TSS<sup>3</sup> to O6K.

Table 2

The MM-GBSA calculations for the best two complexes 8-M<sup>pro</sup> and 9-M<sup>pro</sup> calculated after 100 ns MD simulations utilizing Amber tools 20.

Complex	8-M <sup>pro</sup> complex		9-M <sup>pro</sup> complex	
Residual contribution to the binding	Residues	Binding energy (Kcal/mol)	Residues	Binding energy (Kcal/mol)
	<b>E166</b>	<b>-13.39</b>	<b>D248</b>	<b>-2.50</b>
	<b>LIG</b>	<b>-7.48</b>	<b>LIG</b>	<b>-2.48</b>
	<b>P168</b>	<b>-2.01</b>	P252	-1.28
	M165	-0.87	I249	-1.05
	H172	-0.75	F294	-0.73
	L167	-0.67	V297	-0.44
	F304	-0.47	P293	-0.30
	S602	-0.26	L253	-0.21
	Q189	-0.24	V296	-0.11
	V171	-0.22	L250	-0.10
	T169	-0.11	<b>G251</b>	<b>+0.06</b>
	A173	-0.11	<b>K102</b>	<b>+0.07</b>
	I514	-0.10	<b>R298</b>	<b>+0.07</b>
	<b>D187</b>	<b>+0.10</b>		
	<b>R599</b>	<b>+0.10</b>		
	<b>Q600</b>	<b>+0.10</b>		
	<b>R518</b>	<b>+0.11</b>		
	<b>R188</b>	<b>+0.13</b>		
<b>G170</b>	<b>+0.21</b>			
<b>S139</b>	<b>+0.48</b>			
<b>S302</b>	<b>+1.85</b>			
Binding free energy decomposition				
Complex	8-M <sup>pro</sup> complex		9-M <sup>pro</sup> complex	
$\Delta E_{VDW}$ (kcal/mol)	<b>-27.85</b> ±4.94		<b>-10.37</b> ±5.63	
$\Delta E_{ELE}$ (kcal/mol)	<b>-483.16</b> ±53.41		<b>-290.35</b> ±74.76	
$\Delta G_{GB}$ (kcal/mol)	<b>491.64</b> ±51.77		<b>294.07</b> ±75.60	
$\Delta G_{SA}$ (kcal/mol)	<b>-4.84</b> ±0.69		<b>-2.05</b> ±0.99	
$\Delta G_{GAS}$ (kcal/mol)	<b>-511.02</b> ±55.78		<b>-300.72</b> ±78.96	
$\Delta G_{SOLV}$ (kcal/mol)	<b>486.81</b> ±51.31		<b>292.01</b> ±74.69	
$\Delta G_{TOTAL}$ (kcal/mol)	<b>-24.21</b> ±6.32		<b>-8.70</b> ±5.29	

**Table 3**  
*In silico* prediction of ADME/Tox profiles of the studied compounds.

Comp. No.	MW	#H-bond acceptors	#H-bond donors	Log Po/w (WLOGP)	#Rotatable bonds	TPSA	Lipinski #violations	Ghose #violations	Veber #violations	Solubility Class	GI absorption	BBB Permeant	PAINS	hERG I Inhibitor
(1)	771.11	4	7	0.18	28	184.17	4	3	2	Poorly soluble	Low	No	0 alert	No
(2)	741.04	4	7	-0.33	26	184.17	3	3	2	Poorly soluble	Low	No	0 alert	No
(3)	488.71	4	4	3.41	18	115.83	0	3	1	Moderately soluble	High	No	0 alert	No
(4)	463.68	3	5	1.66	16	115.27	0	2	1	Moderately soluble	High	No	0 alert	No
(5)	486.69	4	4	3.19	17	115.83	0	3	1	Moderately soluble	High	No	0 alert	No
(6)	626.96	2	4	3.24	17	80.44	2	3	1	Poorly soluble	High	No	0 alert	No
(7)	671.01	3	4	4.12	19	91.88	2	3	1	Poorly soluble	High	No	0 alert	No
(8)	671.01	3	4	4.24	19	91.88	2	3	1	Poorly soluble	High	No	0 alert	No
(9)	624.9	4	3	4.63	17	93.61	2	3	1	Poorly soluble	High	No	0 alert	No
(10)	250.4	0	2	1.07	4	27.07	0	0	0	Soluble	High	Yes	0 alert	No
(11)	655.01	2	4	4.02	19	80.44	2	3	1	Poorly soluble	High	No	0 alert	No
(12)	623.94	3	3	4.21	18	81	2	3	1	Poorly soluble	High	No	0 alert	No
(13)	651.99	3	3	4.99	19	81	2	3	1	Poorly soluble	High	No	0 alert	No
(14)	486.69	5	3	4.18	18	118.38	0	3	1	Moderately soluble	High	No	0 alert	No
(15)	640.99	2	4	3.63	18	80.44	2	3	1	Poorly soluble	High	No	0 alert	No

binding energy) for the binding of compound **8** to the M<sup>PRO</sup> (+1.85 kcal/mol). Based on the total binding energy values of the two complexes, the **8**-M<sup>PRO</sup> has lower total binding energy ( $-24.21 \pm 6.32$  kcal/mol) compared to the **9**-M<sup>PRO</sup> ( $-8.70 \pm 5.29$  kcal/mol). Hence, we suggest the effectiveness of compound **8** as a promising inhibitor for hunting the M<sup>PRO</sup> of SARS-CoV-2.

### 3.3. *In silico* prediction of drug-likeness, pharmacokinetics and toxicity (ADME/Tox) profiles

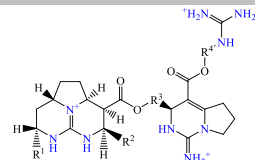
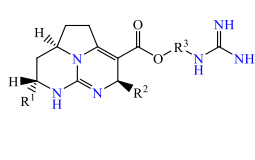
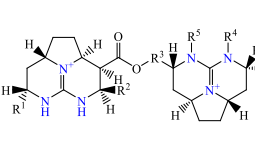
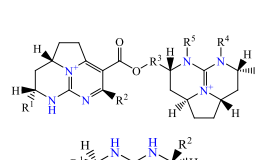
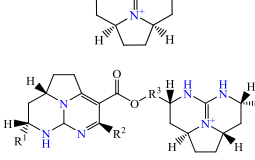
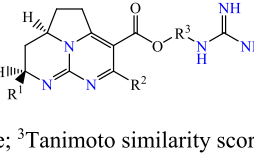
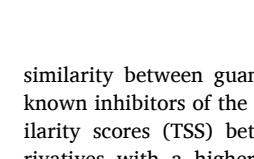
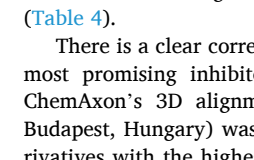
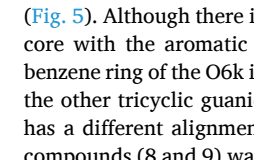
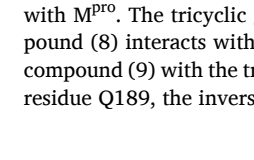


The drug-likeness as well as the pharmacokinetic/toxicological properties for the 15 batzelladine compounds were calculated *in silico* using the SWISS-ADME and pkCSM online webtools and are summarized in Table 3. The MWt of the 15 batzelladines was in the range of 250.4–741.04 with 10 compounds having a MWt of >500 in violation of the Lipinski's rule of 5 for oral drugs. On the other hand, all compounds had between 0 to 5 hydrogen bond acceptors and 2 to 7 hydrogen bond donors. With respect to hydrophobicity, compounds covered a wide spectrum demonstrating a logPo/w between -0.33 to 4.99. Yet, they all lied below the value of 5 which is the cut-off value for oral bioavailability according to Lipinski's rule of five. Furthermore, some compounds had a reasonable number of rotatable bonds and other were highly flexible where compounds had a range of 4–28 rotatable bonds. Looking at the TPSA for this series of compounds, it ranged between 27.07 (for compound **10**) and 184.17 (for compounds **1** and **2**). Applying the drug-likeness filters and starting with the known Lipinski's rule of five, five compounds **3–5**, **10** and **14** showed zero violations, eight compounds demonstrated 2 violations and compounds **1** and **2** showed 4 and 3 violations, respectively, making the latter poor candidates for oral bioavailability. Likewise, applying the Veber and Ghose drug-likeness filters to the new compounds, it was found that with the exception of **10** that demonstrated no violations, all other compounds showed 2 to 3 Ghose violations and 1 to 2 Veber violations.

Further assessment was performed for the pharmacokinetics and toxicity profiles of this series of marine natural alkaloids. First regarding solubility, all the 15 compounds were predicted as being poorly to moderately water soluble except for compound **10** which was predicted to be more soluble than the other 14 batzelladines. Additionally, and with respect to GI absorption, all compounds had a predictable high GI absorption with the exception of compounds **1** and **2** that were predicted to have a low such profile. None of the 15 marine alkaloids exhibited a blood brain barrier permeant ability except derivative **10**, thus can generally be considered free from possible CNS side effects. Also, all guanidinic derivatives had zero PAINS alerts *i.e.*, free from pan-assay interferences. Finally, potential cardiotoxicity of this set of marine alkaloids was assessed through evaluation of their potential hurt to the hERG1 receptor where none of them was found to be a candidate inhibitor for hERG1.

### 3.4. Structure-activity relationship (SAR) studies

The investigated compounds share a common guanidine-containing structure; two of them possess a tricyclic, a bicyclic, and an acyclic guanidinium cores, which are coupled via an ester linkage, (**1**) and (**2**) with predicted free binding energies of -6.54 kcal/mol and -6.36 kcal/mol, respectively, in Table 4. There are eight derivatives that possess two tricyclic guanidinium cores, (**6–9**), (**11–13**) and (**15**) with predicted free binding energies between -7.12 – -6.78 kcal/mol in Table 4. In addition, the derivatives (**10**) and the three derivatives (**3–5**), (**14**) in Table 3, possesses only a tricyclic guanidine-containing core with a predicted free binding energy -5.46 kcal/mol and a tricyclic guanidine-containing core linked to a terminal guanidine by an ester linkage with predicted free binding energies between -6.58 – -6.22 kcal/mol, respectively. Relating the structures (**1–15**; Scheme 1 and 2) to the estimated binding scores (Table 4) suggests that the most influential guanidinium core is the two tricyclic guanidine-containing cores

**Table 4**  
General structure-activity relationship analysis of the tested structurally related cyclic guanidine-containing marine compounds.

No	Guanidinium cores			$\Delta G_B^2$ (kcal/mol)	Chemical Structure	Antiviral activity	TSS <sup>3</sup> to O6K	TSS <sup>3</sup> to N3
	Tricyclic <sup>1</sup>	Bicyclic <sup>1</sup>	Acyclic <sup>1</sup>					
1	Y R <sup>1</sup> =-C <sub>9</sub> H <sub>19</sub> ; R <sup>2</sup> =-CH <sub>3</sub> ; R <sup>3</sup> =-C <sub>8</sub> H <sub>16</sub> -	Y R <sup>4</sup> =-C <sub>4</sub> H <sub>8</sub> -	Y	-6.54		potential	0.228	0.322
2	Y R <sup>1</sup> =-C <sub>7</sub> H <sub>15</sub> ; R <sup>2</sup> =-CH <sub>3</sub> ; R <sup>3</sup> =-C <sub>8</sub> H <sub>16</sub> -	Y R <sup>4</sup> =-C <sub>4</sub> H <sub>8</sub> -	Y	-6.36		potential	0.215	0.337
3	Y R <sup>1</sup> =-C <sub>7</sub> H <sub>15</sub> ; R <sup>2</sup> =-C <sub>3</sub> H <sub>11</sub> ; R <sup>3</sup> =-C <sub>4</sub> H <sub>8</sub> -	N	Y	-6.56		potential	0.223	<b>0.385</b>
4	Y R <sup>1</sup> =-C <sub>9</sub> H <sub>19</sub> ; R <sup>2</sup> =-CH <sub>3</sub> ; R <sup>3</sup> =-C <sub>4</sub> H <sub>8</sub> -	N	Y	-6.58		potential	0.245	0.358
5	Y R <sup>1</sup> =-C <sub>2</sub> H <sub>4</sub> CH=CH-C <sub>3</sub> H <sub>7</sub> ; R <sup>2</sup> =-C <sub>3</sub> H <sub>11</sub> ; R <sup>3</sup> =-C <sub>4</sub> H <sub>8</sub> -	N	Y	-6.56		potential	0.221	0.379
6	Y (two units) R <sup>1</sup> =-C <sub>7</sub> H <sub>15</sub> ; R <sup>2</sup> =-CH <sub>3</sub> ; R <sup>3</sup> =-CH(CH <sub>3</sub> )C <sub>7</sub> H <sub>14</sub> -; R <sup>4</sup> =-H; R <sup>5</sup> =-H	N	N	-6.84		powerful	<b>0.259</b>	0.342
7	Y (two units) R <sup>1</sup> =-C <sub>9</sub> H <sub>19</sub> ; R <sup>2</sup> =-CH <sub>3</sub> ; R <sup>3</sup> =-CH(CH <sub>3</sub> )C <sub>7</sub> H <sub>14</sub> -; R <sup>4</sup> =-OH; R <sup>5</sup> =-H	N	N	-6.84		powerful	<b>0.252</b>	0.329
11	Y (two units) R <sup>1</sup> =-C <sub>9</sub> H <sub>19</sub> ; R <sup>2</sup> =-CH <sub>3</sub> ; R <sup>3</sup> =-CH(CH <sub>3</sub> )C <sub>7</sub> H <sub>14</sub> -; R <sup>4</sup> =-H; R <sup>5</sup> =-H	N	N	-6.78			0.254	0.333
15	Y (two units) R <sup>1</sup> =-C <sub>8</sub> H <sub>17</sub> ; R <sup>2</sup> =-CH <sub>3</sub> ; R <sup>3</sup> =-CH(CH <sub>3</sub> )C <sub>7</sub> H <sub>14</sub> -; R <sup>4</sup> =-H; R <sup>5</sup> =-H	N	N	-6.90		yes	0.256	0.337
8	Y (two units) R <sup>1</sup> =-C <sub>7</sub> H <sub>15</sub> ; R <sup>2</sup> =-CH <sub>3</sub> ; R <sup>3</sup> =-C <sub>7</sub> H <sub>14</sub> -; R <sup>4</sup> =-OH; R <sup>5</sup> =-H	N	N	-7.12		powerful	<b>0.257</b>	0.377
9	Y (two units) R <sup>1</sup> =-C <sub>7</sub> H <sub>15</sub> ; R <sup>2</sup> =-CH <sub>3</sub> ; R <sup>3</sup> =-C <sub>7</sub> H <sub>14</sub> -; R <sup>4</sup> =-H; R <sup>5</sup> =-OH	N	N	-7.00		powerful	<b>0.257</b>	0.250
10	Y R <sup>1</sup> =-C <sub>3</sub> H <sub>11</sub> ; R <sup>2</sup> =-CH <sub>3</sub>	N	N	-5.46			0.194	0.250
12	Y (two units) R <sup>1</sup> =-C <sub>9</sub> H <sub>19</sub> ; R <sup>2</sup> =-CH <sub>3</sub> ; R <sup>3</sup> =-C <sub>7</sub> H <sub>14</sub> -	N	N	-6.80			0.233	0.354
13	Y (two units) R <sup>1</sup> =-C <sub>9</sub> H <sub>19</sub> ; R <sup>2</sup> =-CH <sub>3</sub> ; R <sup>3</sup> =-CH(CH <sub>3</sub> )C <sub>7</sub> H <sub>14</sub> -	N	N	-6.80			0.239	0.346
14	Y R <sup>1</sup> =-C <sub>7</sub> H <sub>15</sub> ; R <sup>2</sup> =-C <sub>3</sub> H <sub>11</sub> ; R <sup>3</sup> =-C <sub>4</sub> H <sub>8</sub> -	N	Y	-6.22			0.223	<b>0.385</b>

<sup>1</sup>Y-Yes and N, No; <sup>2</sup>calculated free binding energies against M<sup>Pro</sup> enzyme; <sup>3</sup>Tanimoto similarity score.

coupled via an ester linkage, as can be seen in the predicted binding scores for the eight derivatives (6–9), (11–13), and (15) in (Table 4).

From those eight derivatives the most promising inhibitors of the M<sup>Pro</sup> enzyme are the derivatives (8) and (9), which have the best predicted free binding energies of  $-7.12$  kcal/mol and  $-7.00$  kcal/mol, respectively. Interestingly, these two derivatives are the only derivatives that possess an aromatic ring embedded in one of the tricyclic guanidinic scaffolds. In general, there appears to be a correlation between the unsaturation in the tricyclic guanidinic scaffold and the calculated binding score, e.g. the derivative (13) is more unsaturated than its partner (11) and has a predicted  $\Delta G_B$  lower than the predicted one for the derivative (11) (Table 4).

However, some care must be taken in this analysis as the same trend is not obtained for the more unsaturated derivative (14) and its partner (3). The hydroxyl substituent in the position R<sup>4</sup> or R<sup>5</sup> also appears to improve the calculated binding score, e.g. the derivative (8) with a N-OH group has a predicted  $\Delta G_B$  lower than that predicted for its partner (6) with a N-H group. The same trend was obtained for the two tricyclic guanidine derivatives (7) and (11). The chemical structure of the most promising derivatives (8) and (9) differs in the position of the hydroxyl group in the tricyclic guanidinic core, at the R<sup>4</sup> or R<sup>5</sup> positions. The calculated binding score is improved for the derivative with a hydroxyl group at the R<sup>4</sup> position (Fig. 4). To compare the structural

similarity between guanidine-containing derivatives (1–15), and the known inhibitors of the M<sup>Pro</sup> enzyme, O6k and N3, the Tanimoto similarity scores (TSS) between them were calculated. Guanidinic derivatives with a higher TSS value were highlighted in **bold blue**, (Table 4).

There is a clear correlation between the highest TSS values and the most promising inhibitors of M<sup>Pro</sup> enzyme for the inhibitor O6k. ChemAxon's 3D alignment tool version 5.7.13.0 (ChemAxon Ltd., Budapest, Hungary) was used to align by extended atom types of derivatives with the highest TSS values (6, 8–9) and the inhibitor O6k, (Fig. 5). Although there is a similar alignment of the tricyclic guanidinic core with the aromatic ring in both compound (8) and (9) with the benzene ring of the O6k inhibitor, as can be seen in Fig. 5, it appears that the other tricyclic guanidine core with alkyl chain in both compounds has a different alignment. The difference in the alignment of the two compounds (8 and 9) was also visualized in Fig. 2 in their binding mode with M<sup>Pro</sup>. The tricyclic guanidine core with the aromatic ring in compound (8) interacts with residue C145 at the active site of M<sup>Pro</sup> and in compound (9) with the tricyclic guanidine core with the alkyl chain. For residue Q189, the inverse situation was observed.

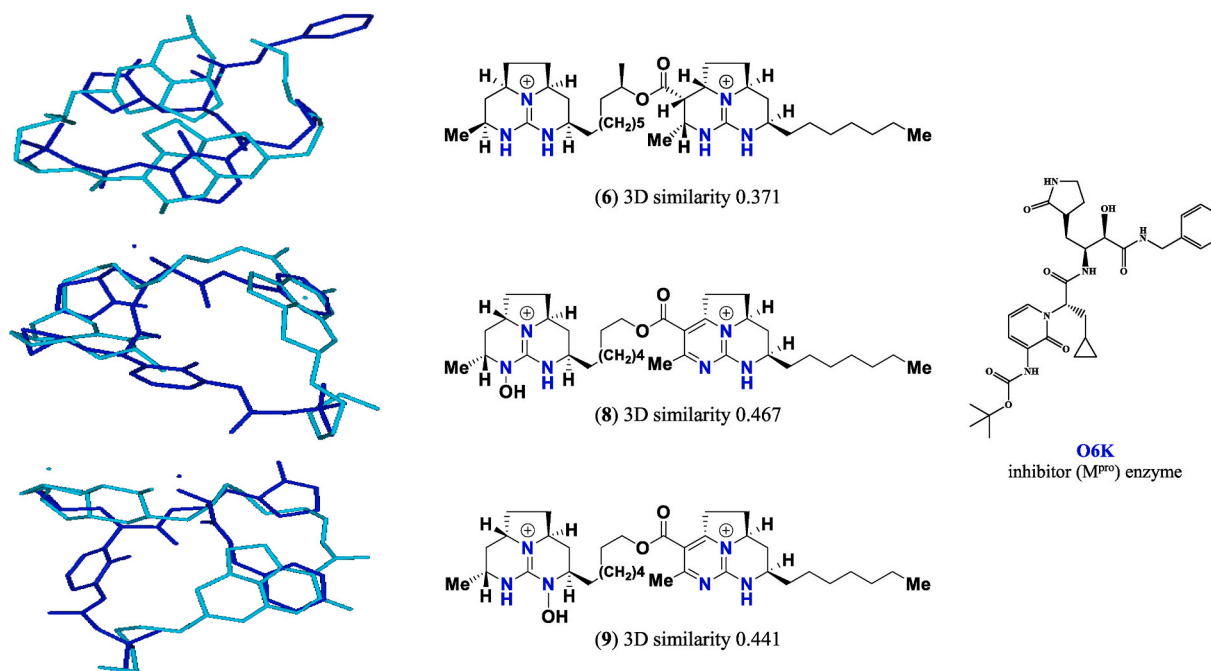


Fig. 5. 3D alignment for the most promising derivatives (6, 8–9) with O6K inhibitor of  $M^{pro}$  enzyme.

#### 4. Conclusions

A focused library of fifteen polycyclic marine batzelladine alkaloids was extensively explored for their binding affinities against the dimeric form of the  $M^{pro}$  of SARS-CoV-2 using a comprehensive package of computational tools involving MDock, MD and SARs studies. MDock simulations revealed that most of the tested compounds are demonstrating very promising binding scores particularly, batzelladines H–I (8–9) which displayed very close binding scores compared to the co-crystallized inhibitor (O6K, positive control). Indeed, the MD simulations showed an advantageous stability for almost of the investigated marine ligands at the ( $M^{pro}$ ) binding site. Furthermore, a preliminary SAR study was accomplished to liaise between different structural features and how far they impacted the proposed activity. Those interesting findings figured out that such distinct molecular architectures are merited and could enlighten the development of promising antiviral leads for paving the COVID-19 pandemic. Moreover, considering the feasible total chemical syntheses for a notable number of these compounds [31,41,82–84] or structurally related congeners could be encouraging for more *in vitro/in vivo* preclinical investigations for COVID-19 control.

#### Funding

Amr El-Demerdash is immensely grateful to the John Innes Centre, Norwich Research Park, United Kingdom for the postdoctoral fellowship. Florbela Pereira would like to thank Fundação para a Ciência e a Tecnologia, MCTES, in the scope of the project UIDB/50006/2020 of the Research Unit, Associate Laboratory for Green Chemistry, LAQV<sup>n</sup>.

#### CRedit authorship contribution statement

**Alaa M. Elgohary:** Formal analysis, Investigation, Resources, Data curation, Writing – original draft, Writing – review & editing. **Abdo A. Elfiky:** Conceptualization, Validation, Formal analysis, Investigation, Resources, Data curation, Writing – original draft, Writing – review & editing. **Florbela Pereira:** Formal analysis, Investigation, Resources, Data curation, Writing – original draft, Writing – review & editing. **Tarek Mohamed Abd El-Aziz:** Investigation, Resources, Writing –

original draft, Writing – review & editing. **Mansour Sobeh:** Investigation, Resources, Writing – original draft, Writing – review & editing. **Reem K. Arafa:** Formal analysis, Investigation, Resources, Data curation, Writing – original draft, Writing – review & editing. **Amr El-Demerdash:** Conceptualization, Validation, Formal analysis, Resources, Data curation, Writing – original draft, Writing – review & editing.

#### Declaration of competing interest

The authors declare that they have no known competing financial interests or personal relationships that could have appeared to influence the work reported in this paper.

#### Acknowledgments

We thank ChemAxon Ltd. for access to JChem and Marvin. Shaheen supercomputer of King Abdullah University of Science and Technology (KAUST) was utilized for MD simulation calculations (under the project number k1482).

#### Appendix A. Supplementary data

Supplementary data to this article can be found online at <https://doi.org/10.1016/j.combiomed.2022.105738>.

#### References

- [1] J.A. Nweze, F.N. Mbaoji, Y.-M. Li, L.-Y. Yang, S.-S. Huang, V.N. Chigor, E.A. Eze, L.-X. Pan, T. Zhang, D.-F. Yang, Potentials of marine natural products against malaria, leishmaniasis, and trypanosomiasis parasites: a review of recent articles, *Infect. Dis. Poverty* 10 (2021) 9.
- [2] W. Bergmann, R.J. Feeney, The isolation of a new thymine pentoside from sponges, *J. Am. Chem. Soc.* 72 (1950) 2809–2810.
- [3] M.F. Stempien, R.F. Nigrelli, G. Pulitzer, Further observations on the caribbean sponge *Cryptotethya crypta* (de Laubenfels), *Nature* 207 (1965), 217–217.
- [4] W. Bergmann, R.J. Feeney, Contributions to the study of marine products. XXXII. The nucleosides of sponges. I, *J. Org. Chem.* 16 (1951) 981–987.
- [5] R. Montaser, H. Luesch, Marine natural products: a new wave of drugs? *Future Med. Chem.* 3 (2011) 1475–1489.
- [6] A. Martins, H. Vieira, H. Gaspar, S. Santos, Marketed marine natural products in the pharmaceutical and cosmeceutical industries: tips for success, *Mar. Drugs* 12 (2014) 1066–1101.

- [7] A.M.S. Mayer, K.B. Glaser, C. Cuevas, R.S. Jacobs, W. Kem, R.D. Little, J. M. McIntosh, D.J. Newman, B.C. Potts, D.E. Shuster, The odyssey of marine pharmaceuticals: a current pipeline perspective, *Trends Pharmacol. Sci.* 31 (2010) 255–265.
- [8] M.A. Ghareeb, M.A. Tammam, A. El-Demerdash, A.G. Atanasov, Insights about clinically approved and Preclinically investigated marine natural products, *Curr. Res. Biotechnol.* 2 (2020) 88–102.
- [9] A.G. Atanasov, S.B. Zotchev, V.M. Dirsch, I.E. Orhan, M. Banach, J.M. Rollinger, D. Barreca, W. Weckwerth, R. Bauer, E.A. Bayer, M. Majeed, A. Bishayee, V. Bochkov, G.K. Bonn, N. Braidy, F. Bucar, A. Cifuentes, G. D'Onofrio, M. Bodkin, M. Diederich, A.T. Dinkova-Kostova, T. Efferth, K. El Bairi, N. Arkells, T.-P. Fan, B. L. Fiebich, M. Freissmuth, M.I. Georgiev, S. Gibbons, K.M. Godfrey, C.W. Gruber, J. Heer, L.A. Huber, E. Ibanez, A. Kijjoo, A.K. Kiss, A. Lu, F.A. Macias, M.J.S. Miller, A. Mocan, R. Müller, F. Nicoletti, G. Perry, V. Pittalà, L. Rastrelli, M. Ristow, G. L. Russo, A.S. Silva, D. Schuster, H. Sheridan, K. Skalicka-Woźniak, L. Skaltsounis, E. Sobarzo-Sánchez, D.S. Bredt, H. Stuppner, A. Sureda, N.T. Tzvetkov, R.A. Vacca, B.B. Aggarwal, M. Battino, F. Giampieri, M. Wink, J.-L. Wolfender, J. Xiao, A.W. K. Yeung, G. Lizard, M.A. Popp, M. Heinrich, I. Berindan-Neogoe, M. Stadler, M. Daglia, R. Verpoorte, C.T. Supuran, T. The International Natural Product Sciences, Natural products in drug discovery: advances and opportunities, *Nat. Rev. Drug Discov.* 20 (2021) 200–216.
- [10] M. Martins, R. Silva, M.M.M. Pinto, E. Sousa, Marine natural products, multitarget therapy and repurposed agents in alzheimer's disease, *Pharmaceuticals* 13 (2020) 242.
- [11] C. Lyu, T. Chen, B. Qiang, N. Liu, H. Wang, L. Zhang, Z. Liu, CMNPD: a comprehensive marine natural products database towards facilitating drug discovery from the ocean, *Nucleic Acids Res.* 49 (2020) D509–D515.
- [12] S.A. Dyshlovoy, F. Honecker, Marine compounds and cancer: updates 2020, *mar. Drugs* 18 (2020) 643.
- [13] C. Jiménez, Marine natural products in medicinal chemistry, *ACS Med. Chem. Lett.* 9 (2018) 959–961.
- [14] C.L. Wainwright, M.M. Teixeira, D.L. Adelson, E.J. Buenz, B. David, K.B. Glaser, Y. Harata-Lee, M.-J. Howes, A.A. Izzo, P. Maffia, Future directions for the discovery of natural product-derived immunomodulating drugs, *Pharmacol. Res.* (2022), 106076.
- [15] X. Ren, X. Xie, B. Chen, L. Liu, C. Jiang, Q. Qian, Marine natural products: a potential source of anti-hepatocellular carcinoma drugs, *J. Med. Chem.* 64 (2021) 7879–7899.
- [16] D.E. Williams, R.J. Andersen, Biologically active marine natural products and their molecular targets discovered using a chemical genetics approach, *Nat. Prod. Rep.* 37 (2020) 617–633.
- [17] A.R. Carroll, B.R. Copp, R.A. Davis, R.A. Keyzers, M.R. Prinsep, *Mar. Nat. Prod. Nat. Prod. Rep.* 37 (2020) 175–223.
- [18] C. Vizetto-Duarte, P. Castelo-Branco, L. Custódio, Marine natural products as a promising source of therapeutic compounds to target cancer stem cells, *Curr. Med. Chem.* 28 (2021) 4343–4355.
- [19] S. Fakhri, A. Yarmohammadi, M. Yarmohammadi, M.H. Farzaei, J. Echeverria, Marine natural products: promising candidates in the modulation of gut-brain Axis towards neuroprotection, *Mar. Drugs* 19 (2021) 165.
- [20] A.R. Carroll, B.R. Copp, R.A. Davis, R.A. Keyzers, M.R. Prinsep, *Mar. Nat. Prod. Nat. Prod. Rep.* 38 (2021) 362–413.
- [21] M. Sebak, F. Molham, M.A. Tammam, A. El-Demerdash, Chemical Diversity and Biological Activities of Anthraquinones Derived from Marine Fungi, A Comprehensive Update, 2022.
- [22] J.A. Nweze, F.N. Mbaoji, Y.-M. Li, L.-Y. Yang, S.-S. Huang, V.N. Chigor, E.A. Eze, L.-X. Pan, T. Zhang, D.-F. Yang, Potentials of marine natural products against malaria, leishmaniasis, and trypanosomiasis parasites: a review of recent articles, *Infect. Dis. Poverty* 10 (2021) 1–19.
- [23] E. Manzo, Synthesis of marine natural products and molecules inspired by marine substances, *Mar. Drugs* 19 (2021) 208.
- [24] W.-Y. Lu, H.-J. Li, Q.-Y. Li, Y.-C. Wu, Application of marine natural products in drug research, *Biorg. Med. Chem.* 35 (2021), 116058.
- [25] J.P. Wong, B. Damania, SARS-CoV-2 dependence on host pathways, *Science* 371 (2021) 884–885.
- [26] M.A. Martínez, Plitidepsin: a repurposed drug for the treatment of COVID-19, *antimicrob. Agents Chemother.* 65 (2021) e00200-00221.
- [27] J.F. Varona, P. Landete, J.A. Lopez-Martin, V. Estrada, R. Paredes, P. Guisado-Vasco, L. Fernandez de Orueta, M. Torralba, J. Fortun, R. Vates, J. Barberan, B. Clotet, J. Ancochea, D. Carnevali, N. Cabello, L. Porras, P. Gijon, A. Monereo, D. Abad, S. Zuñiga, I. Sola, J. Rodon, J. Vergara-Alert, N. Izquierdo-Useros, S. Fudio, M.J. Pontes, B. de Rivas, P. Giron de Velasco, A. Nieto, J. Gomez, P. Avilés, R. Lubomirov, A. Belgrano, B. Sopesen, K.M. White, R. Rosales, S. Yildiz, A.-K. Reuschl, L.G. Thorne, C. Jolly, G.J. Towers, L. Zuliani-Alvarez, M. Bouhaddou, K. Obernier, B.L. McGovern, M.L. Rodriguez, L. Enjuanes, J. M. Fernandez-Sousa, N.J. Krogan, J.M. Jimeno, A. Garcia-Sastre, Preclinical and randomized phase I studies of plitidepsin in adults hospitalized with COVID-19, *Life Sci. Alliance* 5 (2022), e202101200.
- [28] K.M. White, R. Rosales, S. Yildiz, T. Kehrer, L. Miorin, E. Moreno, S. Jangra, M. B. Uccellini, R. Rathnasinghe, L. Coughlan, C. Martinez-Romero, J. Batra, A. Rojic, M. Bouhaddou, J.M. Fabius, K. Obernier, M. Dejoze, M.J. Guillén, A. Losada, P. Avilés, M. Schotsaert, T. Zwaka, M. Vignuzzi, K.M. Shokat, N.J. Krogan, A. Garcia-Sastre, Plitidepsin has potent preclinical efficacy against SARS-CoV-2 by targeting the host protein eIF1A, *Science* 371 (2021) 926–931.
- [29] A. El-Demerdash, A.G. Atanasov, A. Bishayee, M. Abdel-Mogib, J.N.A. Hooper, A. Al-Mourabit, Crambe Batzella, Monanchora, Highly prolific marine sponge genera yielding compounds with potential applications for cancer and other therapeutic areas, *Nutrients* 10 (2018) 33.
- [30] A.E. Demerdash, Isolation of Bioactive Marine Natural Products and Bioinspired Synthesis of Fused Guanidinic Tricyclic Analogues, Université Paris-Saclay (ComUE), 2016.
- [31] A. El-Demerdash, L. Ermolenko, E. Gros, P. Retailleau, B.N. Thanh, G.-B. Anne, A. Al-Mourabit, Short-cut bio-inspired synthesis of tricyclic guanidinic motifs of crambescidins and batzelladines marine alkaloids, *Eur. J. Org. Chem.* (2020) 5677–5684.
- [32] B.B. Snider, W.C. Faith, The total synthesis of (±) - ptilocaulin, *Tetrahedron Lett.* 24 (1983) 861–864.
- [33] S.B.L. Silva, F. Oberhänsli, M.-A. Tribalat, G. Genta-Jouve, J.-L. Teysié, M.-Y. Dechraoui-Bottein, J.-F. Gallard, L. Evanno, E. Poupon, O.P. Thomas, Insights into the biosynthesis of cyclic guanidine alkaloids from crambidae marine sponges, *Angew. Chem. Int. Ed.* 58 (2019) 520–525.
- [34] S. Mai, V. Nagulapalli, A. Patil, A. Truneh, J. Westley, Marine Compounds as HIV Inhibitors, US Patent Application No. WO9301193 (A1), 1993, p. 21.
- [35] A.D. Patil, N.V. Kumar, W.C. Kokke, M.F. Bean, A.J. Freyer, C.D. Brosse, S. Mai, A. Truneh, B. Carte, Novel alkaloids from the sponge *Batzella* sp.: inhibitors of HIV gp120-human CD4 binding, *J. Org. Chem.* 60 (1995) 1182–1188.
- [36] A.D. Patil, A.J. Freyer, P.B. Taylor, B. Carté, G. Zuber, R.K. Johnson, D.J. Faulkner, I. Batzelladines F–, Novel alkaloids from the sponge *Batzella* sp.: inducers of p56lck-CD4 dissociation, *J. Org. Chem.* 62 (1997) 1814–1819.
- [37] H.-M. Hua, J. Peng, D.C. Dunbar, R.F. Schinazi, A.G. de Castro Andrews, C. Cuevas, L.F. Garcia-Fernandez, M. Kelly, M.T. Hamann, Batzelladine alkaloids from the caribbean sponge *Monanchora unguifera* and the significant activities against HIV-1 and AIDS opportunistic infectious pathogens, *Tetrahedron* 63 (2007) 11179–11188.
- [38] L. Kohn, P. Porto, B. Bianchi, M. Santos, R. Berlinck, C. Arns, NOR-Batzelladine L from the sponge *Monanchora* sp. displays antiviral activity against Herpes Simplex virus type 1, *Planta Med.* 78 (2012) CL27.
- [39] A. Olszewski, K. Sato, Z.D. Aron, F. Cohen, A. Harris, B.R. McDougall, W. E. Robinson, L.E. Overman, G.A. Weiss, Guanidine alkaloid analogs as inhibitors of HIV-1 Nef interactions with p53, actin, and p56lck, *Proc. Natl. Acad. Sci. USA* 101 (2004) 14079–14084.
- [40] N. Ahmed, K.G. Brahmabhatt, S.I. Khan, M. Jacob, B.L. Tekwani, S. Sabde, D. Mitra, I.P. Singh, I.A. Khan, K.K. Bhutani, Synthesis and Biological Evaluation of Tricyclic Guanidine Analogues of Batzelladine K for Antimalarial, Antileishmanial, Antibacterial, Antifungal and anti-HIV Activities, *Chemical biology & drug design*, 2012 no-no.
- [41] E.L. Bennett, G.P. Black, P. Browne, A. Hizi, M. Jaffar, J.P. Leyland, C. Martin, I. Oz-Gleenberg, P.J. Murphy, T.D. Roberts, Synthesis and biological activity of analogues of batzelladine F, *Tetrahedron* 69 (2013) 3061–3066.
- [42] C.A. Bewley, S. Ray, F. Cohen, S.K. Collins, L.E. Overman, Inhibition of HIV-1 envelope-mediated fusion by synthetic batzelladine analogues, *J. Nat. Prod.* 67 (2004) 1319–1324.
- [43] F. Zhu, Z. Shi, C. Qin, L. Tao, X. Liu, F. Xu, L. Zhang, Y. Song, X. Liu, J. Zhang, B. Han, P. Zhang, Y. Chen, Therapeutic target database update 2012: a resource for facilitating target-oriented drug discovery, *Nucleic Acids Res.* 40 (2011) D1128–D1136.
- [44] H. Yang, C. Qin, Y.H. Li, L. Tao, J. Zhou, C.Y. Yu, F. Xu, Z. Chen, F. Zhu, Y.Z. Chen, Therapeutic target database update 2016: enriched resource for bench to clinical drug target and targeted pathway information, *Nucleic Acids Res.* 44 (2015) D1069–D1074.
- [45] Y.H. Li, X.X. Li, J.J. Hong, Y.X. Wang, J.B. Fu, H. Yang, C.Y. Yu, F.C. Li, J. Hu, W. W. Xue, Y.Y. Jiang, Y.Z. Chen, F. Zhu, Clinical trials, progression-speed differentiating features and swiftness rule of the innovative targets of first-in-class drugs, *Briefings Bioinf.* 21 (2019) 649–662.
- [46] J. Yang, X. Lin, N. Xing, Z. Zhang, H. Zhang, H. Wu, W. Xue, Structure-based discovery of novel nonpeptide inhibitors targeting SARS-CoV-2 Mpro, *J. Chem. Inf. Model.* 61 (2021) 3917–3926.
- [47] J. Yang, Z. Zhang, F. Yang, H. Zhang, H. Wu, F. Zhu, W. Xue, Computational design and modeling of nanobodies toward SARS-CoV-2 receptor binding domain, *Chem. Biol. Drug Des.* 98 (2021) 1–18.
- [48] X. Wang, F. Li, W. Qiu, B. Xu, Y. Li, X. Lian, H. Yu, Z. Zhang, J. Wang, Z. Li, W. Xue, F. Zhu, SYNBP: synthetic binding proteins for research, diagnosis and therapy, *Nucleic Acids Res.* 50 (2021) D560–D570.
- [49] S. Zhang, K. Amahong, C. Zhang, F. Li, J. Gao, Y. Qiu, F. Zhu, RNA–RNA interactions between SARS-CoV-2 and host benefit viral development and evolution during COVID-19 infection, *Briefings Bioinf.* 23 (2021).
- [50] S. Zhang, K. Amahong, X. Sun, X. Lian, J. Liu, H. Sun, Y. Lou, F. Zhu, Y. Qiu, The miRNA: a small but powerful RNA for COVID-19, *Briefings Bioinf.* 22 (2021) 1137–1149.
- [51] A. El-Demerdash, A.G. Atanasov, O.K. Horbanczuk, M.A. Tammam, M. Abdel-Mogib, J.N.A. Hooper, N. Sekeroglu, A. Al-Mourabit, A. Kijjoo, Chemical diversity and biological activities of marine sponges of the genus *Suberea*: a systematic review, *Mar. Drugs* 17 (2019) 115.
- [52] A. El-Demerdash, C. Moriou, J. Toullac, M. Besson, S. Soulet, N. Schmitt, S. Petek, D. Lecchini, C. Debitus, A. Al-Mourabit, Bioactive bromotyrosine-derived alkaloids from the polynesian sponge *Suberea ianthelliformis*, *Mar. Drugs* 16 (2018) 146.
- [53] A. El-Demerdash, D. Kumla, A. Kijjoo, Chemical diversity and biological activities of meroterpenoids from marine derived-fungi: a comprehensive update, *Mar. Drugs* 18 (2020) 317.
- [54] C. Moriou, D. Lacroix, S. Petek, A. El-Demerdash, R. Trepos, T.M. Leu, C. Florean, M. Diederich, C. Hellio, C. Debitus, Bioactive bromotyrosine derivatives from the



- Pacific marine sponge suberea clavata (Pulitzer-Finali, 1982), *Mar. Drugs* 19 (2021) 143.
- [55] A. El-Demerdash, A.M. Metwaly, A. Hassan, T.M. Abd El-Aziz, E.B. Elkaeed, I. H. Eissa, R.K. Arafa, J.D. Stockand, Comprehensive virtual screening of the antiviral potentialities of marine polycyclic guanidine alkaloids against SARS-CoV-2 (COVID-19), *Biomolecules* 11 (2021) 460.
- [56] A. El-Demerdash, A.A. Al-Karmalawy, T.M. Abdel-Aziz, S.S. Elhady, K.M. Darwish, A.H. Hassan, Investigating the structure-activity relationship of marine natural polyketides as promising SARS-CoV-2 main protease inhibitors, *RSC Adv.* 11 (2021) 31339–31363.
- [57] A. El-Demerdash, A. Hassan, T.M. Abd El-Aziz, J.D. Stockand, R.K. Arafa, Marine brominated tyrosine alkaloids as promising inhibitors of SARS-CoV-2, *Molecules* 26 (2021) 6171.
- [58] A.H. Arshia, S. Shadravan, A. Solhjoo, A. Sakhteman, A. Sami, De novo design of novel protease inhibitor candidates in the treatment of SARS-CoV-2 using deep learning, docking, and molecular dynamic simulations, *Comput. Biol. Med.* 139 (2021), 104967.
- [59] M. Jomhori, H. Mosaddeghi, H. Farzin, Tracking the interaction between single-wall carbon nanotube and SARS-Cov-2 spike glycoprotein: a molecular dynamics simulations study, *Comput. Biol. Med.* 136 (2021), 104692.
- [60] S. Murugesan, S. Kottekad, I. Crasta, S. Sreevathsan, D. Usharani, M.K. Perumal, S. N. Mudliar, Targeting COVID-19 (SARS-CoV-2) main protease through active phytochemicals of ayurvedic medicinal plants - *Emblca officinalis* (Amla), *Phyllanthus niruri* Linn. (Bhumi Amla) and *Tinospora cordifolia* (Giloy) - a molecular docking and simulation study, *Comput. Biol. Med.* 136 (2021), 104683.
- [61] W. Xue, F. Yang, P. Wang, G. Zheng, Y. Chen, X. Yao, F. Zhu, What contributes to serotonin-norepinephrine reuptake inhibitors' dual-targeting mechanism? The key role of transmembrane domain 6 in human serotonin and norepinephrine transporters revealed by molecular dynamics simulation, *ACS Chem. Neurosci.* 9 (2018) 1128–1140.
- [62] W. Xue, T. Fu, S. Deng, F. Yang, J. Yang, F. Zhu, Molecular mechanism for the allosteric inhibition of the human serotonin transporter by antidepressant Escitalopram, *ACS Chem. Neurosci.* 13 (2022) 340–351.
- [63] D.A. Evans, History of the harvard ChemDraw project, *Angew. Chem. Int. Ed.* 53 (2014) 11140–11145.
- [64] M.D. Hanwell, D.E. Curtis, D.C. Lonie, T. Vandermeersch, E. Zurek, G.R. Hutchison, Avogadro: an advanced semantic chemical editor, visualization, and analysis platform, *J. Cheminf.* 4 (2012) 17.
- [65] A.K. Rappe, C.J. Casewit, K.S. Colwell, W.A. Goddard, W.M. Skiff, UFF, a full periodic table force field for molecular mechanics and molecular dynamics simulations, *J. Am. Chem. Soc.* 114 (2002) 10024–10035.
- [66] Z. Bikadi, E. Hazai, Application of the PM6 semi-empirical method to modeling proteins enhances docking accuracy of AutoDock, *J. Cheminf.* 1 (2009) 15.
- [67] L. Zhang, D. Lin, X. Sun, U. Curth, C. Drost, L. Sauerhering, S. Becker, K. Rox, R. Hilgenfeld, Crystal structure of SARS-CoV-2 main protease provides a basis for design of improved  $\alpha$ -ketoamide inhibitors, *Science* 368 (2020) 409–412.
- [68] Z. Jin, X. Du, Y. Xu, Y. Deng, M. Liu, Y. Zhao, B. Zhang, X. Li, L. Zhang, C. Peng, Y. Duan, J. Yu, L. Wang, K. Yang, F. Liu, R. Jiang, X. Yang, T. You, X. Liu, X. Yang, F. Bai, H. Liu, X. Liu, L.W. Guddat, W. Xu, G. Xiao, C. Qin, Z. Shi, H. Jiang, Z. Rao, H. Yang, Structure of Mpro from SARS-CoV-2 and discovery of its inhibitors, *Nature* 582 (2020) 289–293.
- [69] G.M. Morris, R. Huey, W. Lindstrom, M.F. Sanner, R.K. Belew, D.S. Goodsell, A. J. Olson, AutoDock4 and AutoDockTools4: automated docking with selective receptor flexibility, *J. Comput. Chem.* 30 (2009) 2785–2791.
- [70] O. Trott, A.J. Olson, AutoDock Vina, improving the speed and accuracy of docking with a new scoring function, efficient optimization, and multithreading, *J. Comput. Chem.* 31 (2010) 455–461.
- [71] J.C. Phillips, R. Braun, W. Wang, J. Gumbart, E. Tajkhorshid, E. Villa, C. Chipot, R. D. Skeel, L. Kale, K. Schulten, Scalable molecular dynamics with NAMD, *J. Comput. Chem.* 26 (2005) 1781–1802.
- [72] J. Huang, A.D. MacKerell Jr., CHARMM36 all-atom additive protein force field: validation based on comparison to NMR data, *J. Comput. Chem.* 34 (2013) 2135–2145.
- [73] M.F. Harrach, B. Drossel, Structure and dynamics of TIP3P, TIP4P, and TIP5P water near smooth and atomistic walls of different hydrophobicity, *J. Chem. Phys.* 140 (2014), 174501.
- [74] P. Mark, L. Nilsson, Structure and dynamics of the TIP3P, SPC, and SPC/E water models at 298 K, *J. Phys. Chem.* 105 (2001) 9954–9960.
- [75] W. Humphrey, A. Dalke, K. Schulten, VMD: visual molecular dynamics, *J. Mol. Graph.* 14 (33–38) (1996) 27–38.
- [76] E.F. Pettersen, T.D. Goddard, C.C. Huang, G.S. Couch, D.M. Greenblatt, E.C. Meng, T.E. Ferrin, UCSF Chimera—a visualization system for exploratory research and analysis, *J. Comput. Chem.* 25 (2004) 1605–1612.
- [77] S. Genheden, U. Ryde, The MM/PBSA and MM/GBSA methods to estimate ligand-binding affinities, *Expert Opin. Drug Discov.* 10 (2015) 449–461.
- [78] A. Daina, O. Michielin, V. Zoete, SwissADME: a free web tool to evaluate pharmacokinetics, drug-likeness and medicinal chemistry friendliness of small molecules, *Sci. Rep.* 7 (2017) 42717.
- [79] J.B. Baell, G.A. Holloway, New substructure filters for removal of Pan assay interference compounds (PAINS) from screening libraries and for their exclusion in bioassays, *J. Med. Chem.* 53 (2010) 2719–2740.
- [80] D.E.V. Pires, T.L. Blundell, D.B. Ascher, pkCSM, Predicting small-molecule pharmacokinetic and toxicity properties using graph-based signatures, *J. Med. Chem.* 58 (2015) 4066–4072.
- [81] E. Sfecci, T. Lacour, P. Amade, M. Mehiri, Polycyclic guanidine alkaloids from *Poecilosclerida* marine sponges, *Mar. Drugs* 14 (2016) 77.
- [82] Y.-C. Lin, A. Ribaucourt, Y. Moazami, J.G. Pierce, Concise synthesis and antimicrobial evaluation of the guanidinium alkaloid batzelladine D: development of a stereodivergent strategy, *J. Am. Chem. Soc.* 142 (2020) 9850–9857.
- [83] Y. Guo, Z. Gao, G. Huang, H. Zhong, X. Meng, H. Tang, C. Zou, Synthesis of the chiral intermediate of batzelladines A and B, *ps* 192 (2017) 113–117.
- [84] N.R. Babji, J.P. Wolfe, Asymmetric total synthesis of (+)-Merobatzelladine B, *Angew. Chem. Int. Ed.* 51 (2012) 4128–4130.